Impact of molecular chlorine production from aerosol iron photochemistry on atmospheric oxidative capacity in North China

Qianjie Chen[1,], Xuan Wang[2], Xiao Fu[3], Xinxin Li[1], Becky Alexander[4], Xiang Peng[1,‡], Weihao Wang[1,♀], Men Xia[1,†], Yue Tan[1], Jian Gao[5], Jianmin Chen[6], Yujing Mu[7], Pengfei Liu[7], and Tao Wang[1,*]*

[1] Department of Civil and Environmental Engineering, The Hong Kong Polytechnic University, Hong Kong SAR, China

[2] School of Energy and Environment, City University of Hong Kong, Hong Kong SAR, China

[3] Institute of Environment and Ecology, Tsinghua Shenzhen International Graduate School, Tsinghua University, Shenzhen 518055, China

[4] Department of Atmospheric Sciences, University of Washington, Seattle, Washington, USA

[5] State Key Laboratory of Environmental Criteria and Risk Assessment, Chinese Research Academy of Environmental Sciences, Beijing 100084, China

[6] Department of Environmental Science and Engineering and Institute of Atmospheric Sciences, Fudan University, Shanghai 200433, China

[7] Research Center for Eco-Environmental Sciences, Chinese Academy of Sciences, Beijing 100085, China

Abstract. Elevated levels of atmospheric molecular chlorine (Cl_2) have been observed during daytime in recent field studies in China, but could not be explained by the current chlorine chemistry mechanisms in models. Here we propose a Cl_2 formation mechanism initiated by aerosol iron photochemistry to explain the daytime Cl_2 formation. We implement this mechanism into the GEOS-Chem chemical transport model, and investigate its impacts on atmospheric composition in wintertime North China where high levels of Cl_2 as well as aerosol chloride and iron were observed. The new mechanism accounts for more than 90% of surface air Cl_2 production in North China, and consequently increases the surface air Cl_2 abundances by an order of magnitude, improving the model's agreement with observed Cl_2. The presence of high Cl_2 significantly alters the oxidative capacity of the atmosphere, with a factor of 20 to 40 increase in chlorine radical concentration and 20% to 40% increase in hydroxyl radical concentration in regions with high aerosol chloride and iron loadings. This results in an increase of surface air ozone by about 10%. This new Cl_2 formation mechanism will improve model simulation capability for reactive chlorine abundances in the regions with high emissions of chlorine and iron.

Keywords. Molecular chlorine, Iron, Chloride, Aerosol photochemistry, GEOS-Chem

Synopsis. The mechanism through which molecular chlorine reaches elevated daytime levels in North China remains unclear. This study suggests aerosol iron photochemistry as the main mechanism, with implications for air quality.

1. Introduction

Chlorine radicals (Cl) are strong oxidants in the atmosphere and can contribute to the formation of ozone (O_3) and secondary organic aerosols (SOA) through oxidizing volatile organic compounds (VOCs). [1-5] In addition, their reactions with greenhouse gases methane (CH_4) and O_3 and sulfate aerosol precursor dimethyl sulfide (DMS) in the troposphere have climate implications.[1,6-8,72,73] Chlorine radicals are generated through photochemical chlorine chemistry during daytime, involving a variety of chlorine species such as molecular chlorine (Cl_2), hypochlorous acid (HOCl), nitryl chloride ($ClNO_2$), chlorine nitrate ($ClNO_3$), hydrogen chloride (HCl), and chlorine monoxide (ClO).[9,10] Over the past two decades, research has focused on $ClNO_2$ as a large source of chlorine radicals upon photolysis in the morning over both coastal and inland regions.[11-13] Recently, high levels of Cl_2 (tens to hundreds of ppt) were observed during daytime at multiple sites in China,[14-18] indicating that Cl_2 could serve as a significant daytime source of chlorine radicals in the polluted environments, especially in the afternoon when $ClNO_2$ levels become low.

The main Cl_2 formation mechanisms in the troposphere are generally thought to be the reactions of $ClNO_3$, $ClNO_2$, HOCl, and hydroxyl radicals (OH) with chloride on aerosols.[1,10,17]

Recently, Peng et al. [15] proposed photodissociation of aerosol nitrate as the dominant source of daytime Cl_2 observed in Hong Kong, which has not been included in the chemical transport model. Cl_2 is photolyzed rapidly under sunlight and is therefore hard to accumulate during daytime (lifetime < 10 minutes around noon at mid-latitudes). Previous modeling studies with the available gas-phase and multiphase Cl_2 formation mechanisms have shown difficulties in reproducing daytime Cl_2 observations in the field.[4,9,17,19] In particular, Wang et al.[9] showed that the GEOS-Chem chemical transport model with detailed gas-phase and multiphase chlorine chemistry scheme could not reproduce 1-2 ppt of daytime Cl_2 observed during the WINTER aircraft campaign over Eastern US. Further, Chen et al.[17] used a box model with comprehensive observational constraints and found the traditional Cl_2 formation mechanisms underestimated the observed Cl_2 by almost one order of magnitude around noon at a suburban site in East China. They proposed aerosol photochemistry, involving iron (Fe) for example, as the daytime Cl_2 missing source, based on the correlation between daytime Cl_2 missing source with sunlight intensity and aerosol abundance.[17]

Indeed, previous laboratory studies have observed efficient Cl_2 production from photolysis of aerosols or salt particles containing Fe(III) and chloride, and proposed Fe(III)-induced aerosol photochemistry to account for Cl_2 production (*R*1-*R*11).[20,21] Based on ab initio calculations, Mikkelsen et al.[74] found that $FeCl^{2+}$ would not undergo photodissociation by sunlight at the Earth's surface. They suggested $FeCl_2^+$ as the most important species for $Cl_{(aq)}$ production while $FeCl_3$ and $FeCl_4^-$ could also contribute to $Cl_{(aq)}$ production under typical atmospheric conditions at the Earth's

surface.[74] Recently, van Herpen et al.[22] further proposed aerosol iron photochemistry as the dominant source of Cl_2 over North Atlantic where Sahara dust mixes with sea spray aerosol. In addition, the Fe(III)-induced photolytic Cl_2 formation was proposed as a method for industrial water disinfection and waste water treatment[23] and a geo-engineering method to remove greenhouse gas methane (CH_4).[24,25] Nevertheless, the impacts of Cl_2 produced through aerosol iron photochemistry on the atmospheric composition over regions with high anthropogenic emissions are yet to be investigated in a chemical transport model.

$$FeCl^{2+} + h\nu \rightarrow Fe^{2+} + Cl_{(aq)} \quad (R1)$$

$$FeCl_2^{+} + h\nu \rightarrow FeCl^{+} + Cl_{(aq)} \quad (R2)$$

$$FeOH^{2+} + h\nu \rightarrow Fe^{2+} + OH_{(aq)} \quad (R3)$$

$$Fe(OH)_2^{+} + h\nu \rightarrow FeOH^{+} + OH_{(aq)} \quad (R4)$$

$$Cl_{(aq)} + Cl^{-} \rightleftharpoons Cl_2^{-} \quad (R5)$$

$$Cl_{(aq)} + Cl_2^{-} \rightleftharpoons Cl^{-} + Cl_2 \quad (R6)$$

$$Cl_2^{-} + Cl_2^{-} \rightarrow Cl_3^{-} + Cl^{-} \quad (R7)$$

$$Cl_3^{-} \rightleftharpoons Cl_2 + Cl^{-} \quad (R8)$$

$$OH_{(aq)} + Cl^{-} \rightleftharpoons ClOH^{-} \quad (R9)$$

$$ClOH^{-} + H^{+} \rightleftharpoons ClOH_{2(aq)} \quad (R10)$$

$$ClOH_{2(aq)} \rightarrow Cl_{(aq)} + H_2O \quad (R11)$$

In this study, the aerosol Fe(III)-induced photolytic Cl_2 formation mechanism was implemented into the GEOS-Chem chemical transport model for the first time, and the impacts on reactive chlorine budget, atmospheric oxidative capacity, and air quality in the North China domain were assessed. This work highlights the potential of aerosol iron photochemistry serving as a significant daytime Cl_2 source in polluted environments and the need for more studies to better quantify this source and the impacts on air quality in regions with high chlorine and iron emissions.

2. Method

2.1 GEOS-Chem model

We used the GEOS-Chem chemical transport model v12.9.3 with coupled ozone–NOx–VOCs–aerosol–halogen chemistry[9]. The nested-grid version of the model has a horizontal resolution of 0.25°×0.3125° over East Asia and 47 vertical levels (120-150 m thickness for the first 12 layers) up to 0.01 hPa. We focus on the North China study domain ([110°-123.75°E, 30°-42.25°N]) where concurrent field measurements of reactive chlorine and aerosol iron and chloride were performed. The model is driven by GEOS-FP (forward processing) assimilated meteorological data from the NASA Global Modeling and Assimilation Office (GMAO). The boundary conditions were obtained from a global model run with 4°×5° horizontal resolution after one-year spin up. The spin-up time for the nested-grid model runs was one month.

The GEOS-Chem model has an extensive halogen chemistry scheme, including comprehensive gas-phase and multiphase chlorine, bromine, and iodine reactions, as described in details in previous studies.[9,26-28] Briefly, the model considers 12 gas-phase inorganic chlorine species (Cl, ClO, ClOO, OClO, $ClNO_2$, $ClNO_3$, HOCl, BrCl, ICl, HCl, Cl_2, Cl_2O_2) and aerosol chloride at 2 size ranges (fine-mode <1 μm diameter and coarse mode >1 μm diameter). The equilibrium between HCl and fine-mode aerosol chloride is calculated with ISORROPIA II thermodynamic equilibrium module implemented in GEOS-Chem.[2,29] The gas-phase and multiphase Cl_2 formation mechanisms used in our model are shown in Table S1. The gas-phase Cl_2 formation mechanisms include $ClNO_3$ + Cl, ClO + ClO, and ClOO + Cl reactions. The multiphase Cl_2 formation mechanisms include uptake of $ClNO_3$, HOCl, $ClNO_2$, and OH by chloride-containing aerosols.

The Multiresolution Emission Inventory for China (MEIC) with a horizontal resolution of 0.25°×0.25° was used for Chinese anthropogenic emissions other than chlorine. The anthropogenic emissions of HCl and fine-mode aerosol Cl^- over China with a horizontal resolution of 0.1°×0.1° were added to the model, following a recent GEOS-Chem modeling study for the year 2014.[2,30] We applied annual scaling factors for coal combustion and industrial sources based on the MEIC inventory,[31] agricultural fires and residential biofuel sources based on the MODIS fire radiative energy data,[32] and waste incineration sources based on the Chinese statistical data (National Bureau of Statistics: www.stats.gov.cn; last access: 05/03/2024). The total anthropogenic emissions of HCl and fine-mode Cl^- over China were simulated to be 827 Gg Cl a^{-1} in 2017 (129

Gg Cl a^{-1} from coal combustion and industrial processes, 299 Gg Cl a^{-1} from agricultural fires and residential biofuel, and 399 Gg Cl a^{-1} from waste incineration), compared to 932 Gg Cl a^{-1} in 2013 (174 Gg Cl a^{-1} from coal combustion and industrial processes, 507 Gg Cl a^{-1} from agricultural fires and residential biofuel, and 251 Gg Cl a^{-1} from waste incineration).[2] Sea salt Cl^- emissions were based on Wang et al.[2,10] The fine-mode aerosol chloride concentration over China during the study period (December 9-31, 2017) is shown in Figure 1, with 8±6 μg m^{-3} simulated for the 29 sampling sites in North China compared to 6±3 μg m^{-3} observed.

The Fe(III)-induced photolytic Cl_2 formation mechanism was implemented into the model, based on previous chamber experimental results.[20] Only fine-mode aerosols were considered to initiate Fe(III)-induced photolytic Cl_2 production, as they were used in the chamber experiments[20] and fine-mode aerosols have longer lifetime that allows Fe^{3+} and Cl^- to mix in the aerosols.[33,34] The production rate of Cl_2 ($d[Cl_2]/dt$: cm^{-3} s^{-1}) was assumed to be a function of NO_2 photolysis frequency (j_{NO2}: s^{-1}), aerosol Fe(III) concentration ($[Fe^{3+}]$: mol l^{-1}), aerosol chloride concentration ($[Cl^-]$: mol l^{-1}), and aerosol surface area concentration (S: μm^2 cm^{-3}), as shown in $E1$.

$$\frac{d[\mathrm{Cl}_2]}{dt} = \alpha j_{NO2}[Fe^{3+}][Cl^-]S \qquad (E1)$$

where α (=1.4×10^5 μm^{-2} M^{-2}) is a scaling factor obtained based on previous experimental results[20] (*Supplementary Information Text S1*). j_{NO2} was used to represent sunlight intensity, as it was reported in the experiments.[20] The dependence of Cl_2 production rate on aerosol surface area concentration follows Wittmer et al.[20], but more experiments are needed to investigate this effect in the future. Both anthropogenic Fe and mineral dust Fe are simulated in the model, following

previous GEOS-Chem modeling studies.[35,36] Anthropogenic emission of Fe ($[Fe]_{ant}$) was assumed to be 1/30 of anthropogenic primary sulfate emission due to their similar sources (power plants, industry, residential and transportation), and mineral dust Fe ($[Fe]_{dust}$) was assumed to be 3.5% of total dust mass.[35] Mineral dust includes both natural dust in four size bins (radius of 0.1–1.0, 1.0–1.8, 1.8–3.0, and 3.0–6.0 μm) and anthropogenic dust released from road, residential, and commercial construction and combustion in one size bin (radius of 0.1–1.0 μm).[37] In the default GEOS-Chem setup, the soluble fraction of Fe was assumed to be 10% for $[Fe]_{ant}$ and 1% for $[Fe]_{dust}$.[35] The soluble fraction of $[Fe]_{ant}$ was found to vary from 0.06%-81% in previous studies.[38,39] In previous laboratory experiments, the soluble fraction of Fe reaches 74% for oil fly ash, 4% for coal fly ash, 26% for biomass burning aerosols, and 4% for Chinese loess (from Shanxi) after 12 h in acidic solution, suggesting an increase of iron solubility when aerosols undergo chemical processing during atmospheric transport.[40] In order to better match $PM_{2.5}$ soluble Fe observations at Beijing [40.00°N, 116.35°E] and Handan [36.57°N, 114.50°E] during part of the study period,[41] we increased the solubilities of $[Fe]_{ant}$ and $[Fe]_{dust}$ by a factor of 4, resulting in 31% model underestimation in Beijing and 69% model overestimation in Handan (Table S2). The Fe^{3+} fraction of soluble Fe ($f_{Fe3+} = Fe^{3+}/(Fe^{3+} + Fe^{2+})$) was assumed to be 67% during daytime, based on the aerosol samples collected from the Asian continental outflow during daytime (67±8%)[33] and loess samples collected from the Shanxi region of the Chinese loess plateau (67%).[42] Note that f_{Fe3+} in ambient aerosols could be highly variable (0~100%), due to a series of complex processes involving sunlight, oxidizing compounds (e.g. HO_2, O_2^-, H_2O_2, O_3), and ligands (e.g. oxalate,

formate).[43,44] More field observations are needed in the future to better constrain f_{Fe3+} in different environments. The speciation of Fe depends on aerosol acidity, which is discussed in Section 3.5. Sulfate and organics in the aerosols were found to suppress Fe(III)-induced photolytic Cl_2 production[21], as discussed in Section 3.5. The acidity and suppression effects are not considered in this study and should be further quantified through laboratory experiments in the future.

The mechanisms for aromatic chemistry developed by Bates et al.[45] and C_2H_4 and C_2H_2 chemistry developed by Kwon et al.[46] were implemented into the model. Following Wang et al.,[2] formation of secondary organic aerosols (SOA) from oxidation of VOCs by Cl radicals is not included in the model due to large uncertainties involved in these processes. The GEOS-Chem default "simple SOA" scheme was used, which assumes that SOA are produced from anthropogenic and biogenic volatile organic precursors on a timescale of one day with fixed yields.[47,48] The "simple SOA" scheme has shown good ability to simulate organic aerosol observations globally.[48, 49] Following Shah et al.,[50] we used $\gamma_{NO2}=1\times10^{-5}$ for aerosol uptake of NO_2 to better simulate HONO and NO_2 in North China. Following Jaegle et al.,[51] we assumed HONO as the only product of aerosol uptake of NO_2, to be consistent with laboratory studies showing that HONO is the main product especially under sunlight and some formation of the absorbed HNO_3 could be released back as NO_2 or NO.[52-54]

2.2 Observational data

A field campaign was conducted at the SRE-RCEES station ([38.66°N, 115.25°E], Fig. 1a) in Wangdu County during December 9-31, 2017.[14] The sampling site located in an agricultural field that could be impacted by emissions from road traffic and rural household coal burning for heating and cooking. During the campaign, reactive halogens and other trace gases as well as aerosols and meteorological parameters were measured. Cl_2 was measured with an iodide-adduct quadrupole chemical ionization mass spectrometer (Q-CIMS, THS Instruments, GA, USA), with a detection limit of 3 ppt and an uncertainty of 25%.[14] The isotopic ratio (*m/z* 199 vs. *m/z* 197) of the ambient Cl_2 signals (0.63) was in good agreement with the natural abundance (0.65).[14] $PM_{2.5}$ total iron (Fe) concentration was measured by an elemental analyzer (Xact 625i, CES), using energy dispersive X-ray fluorescence technique with a time resolution of one hour. $PM_{2.5}$ Cl^-, as well as SO_4^{2-}, NO_3^-, NH_4^+ and organics, were measured by a Time of Flight-Aerosol Chemical Speciation Monitor (Tof-ACSM, Aerodyne Inc.). Other measurements during the field campaign include j_{NO2}, aerosol size distribution and number concentrations, temperature (*T*), relative humidity (RH), O_3, NO_2, NO, NH_3, SO_2 and CO mixing ratios, which have been described in Peng et al.[14] The wet aerosol surface area concentration was calculated in Peng et al. [14] considering the chemical composition-based aerosol hygroscopicity in the North China region[69] and RH-dependent growth factors[70]. During the study period (December 9-31, 2017), $PM_{2.5}$ samples were collected daily at 28 sites in North China ("2+26" cities) from 9 a.m. to 8 a.m. next day.[55] The locations of the 28 $PM_{2.5}$ sampling sites and the Wangdu site are shown in Figure 1a. The total iron concentrations in the $PM_{2.5}$ samples were measured with inductively coupled plasma mass spectrometry (ICP-MS,

Agilent Technologies), with a low detection limit (0.003 μg m^{-3}). The Cl^-, SO_4^{2-}, NO_3^-, NH_4^+ concentrations in the $PM_{2.5}$ samples were measured with ion chromatography, with low detection limits ranging from 0.003 to 0.032 μg m^{-3}.[55]

3. Results and Discussion

3.1 Aerosol chloride and iron abundances

Figure 1a shows the average fine-mode aerosol chloride mass concentration ($[Cl^-]$) in surface air over the North China domain during the study period (December 9-31) in the model run considering aerosol iron photochemistry (RUN_{Fe}). Hot spots of aerosol chloride are expected in the central region (Hebei, Hubei, and Shandong Provinces) due to anthropogenic emissions from coal combustion, biomass burning, and waste burning, as discussed in Fu et al.[30] and Wang et al.[2] The model (RUN_{Fe}) is able to reproduce the spatial and daily variabilities of $[Cl^-]$ (Fig. 1). The average modeled $[Cl^-]$ is 8.3±5.7 μg m^{-3} for the 29 sampling sites in North China during the study period, on average 50% higher than observed $PM_{2.5}$ $[Cl^-]$ (5.6±3.1 μg m^{-3}) ($p < 0.01$). The model overestimation of $[Cl^-]$ mainly occurred during $PM_{2.5}$ episodes around December 14, 22, and 28 when $PM_{2.5}$ concentrations were also overestimated by the model (Fig. 1c). The model-observation discrepancy for individual sites is generally within a factor of two (Fig. 1b). In addition, the diurnal variability of $[Cl^-]$ at the Wangdu site is reproduced by the model (Fig. 4c), with higher concentrations at night and lower concentrations during daytime due to ventilation in the atmospheric boundary layer. Considering the limited knowledge of anthropogenic chlorine

emission inventory in China[3,30,71], our model seems to reasonably simulate observed [Cl^-] in North China during the study period.

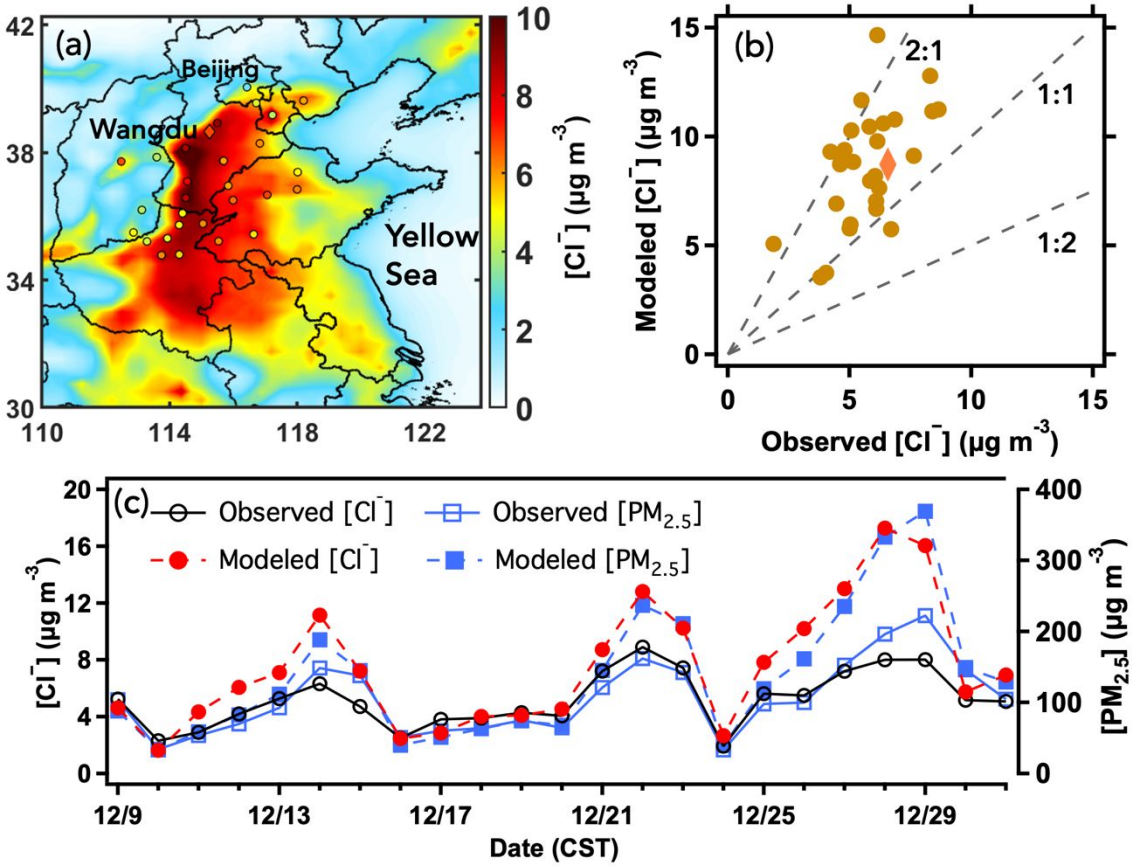

Figure 1. (a) Modeled (RUN_{Fe}) fine-mode aerosol chloride concentrations ([Cl^-]) in North China overplotted with observed $PM_{2.5}$ [Cl^-] at 29 sites, both averaged during the study period (December 9-31, 2017). (b) Scatter plot of modeled versus observed [Cl^-] for the 29 sites in North China shown in (a), with three dashed lines as 2:1, 1:1, and 1:2 ratios. (c) Daily variability of the observed and modeled [Cl^-] and [$PM_{2.5}$] for the 29 sites averaged in North China during December 9-31. The Wangdu site is highlighted as a diamond symbol in (a) and (b).

During the study period, the total Fe concentration was measured for $PM_{2.5}$ samples collected at 29 sites in North China, with an average of 1.0±0.7 μg m^{-3}. In comparison, the total Fe mass concentration of $PM_{2.0}$ (diameter < 2 μm, size of fine-mode dust in GEOS-Chem[37]) is modeled to be 0.9±0.5 μg m^{-3} on average for the 29 sites in North China during the study period in RUN_{Fe}, similar to observations (Fig. 2). Our model shows relatively good performance for $[Fe]_{tot}$ compared to a previous study with 40% model-observation discrepancy in North China[36]. The daily and diurnal variabilities of total Fe are generally reproduced by the model (Figs. 2c and 4d). The discrepancy between modeled and observed total Fe is generally within a factor of two (Fig. 2b). During part of the study period (December 21-31, 2017), the soluble Fe concentrations were measured for $PM_{2.5}$ collected at Beijing and Handan,[41] which are about 150 km to the northeast and 250 km to the southwest of the Wangdu site, respectively. The solubility of aerosol Fe is on average 4.6% in Beijing and 4.5% in Handan observed, compared to 5.7% in Beijing and 6.6% in Handan modeled. The aerosol soluble Fe concentration is underestimated by 31% in Beijing and overestimated by 69% in Handan in the model due to the discrepancy between modeled and observed aerosol total Fe at these two sites (Table S2).

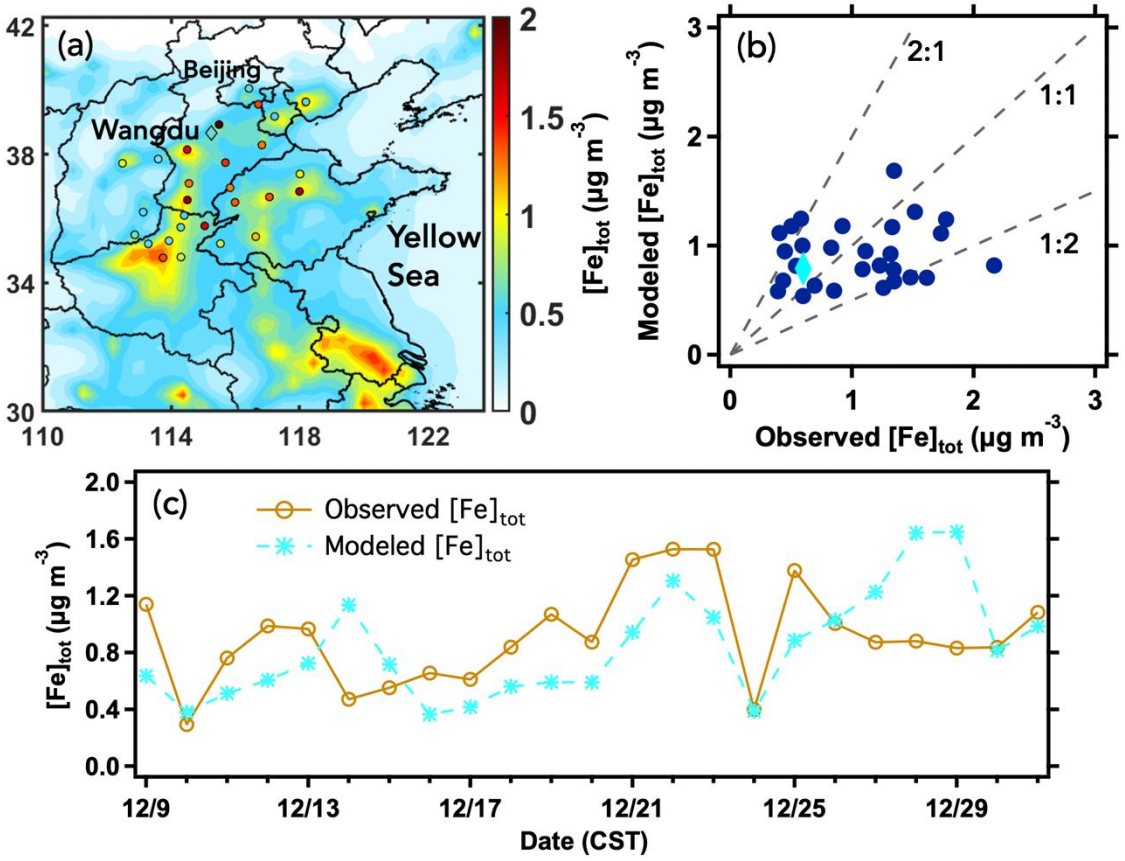

Figure 2. (a) Modeled (RUN_{Fe}) fine-mode aerosol total Fe concentrations ($[Fe]_{tot}$) in North China overplotted with observed $PM_{2.5}$ $[Fe]_{tot}$ at 29 sites, both averaged during the study period (December 9-31, 2017). (b) Scatter plot of modeled versus observed $[Fe]_{tot}$ for the 29 sites in North China shown in (a), with three dashed lines as 2:1, 1:1, and 1:2 ratios. (c) Daily variability of the observed and modeled $[Fe]_{tot}$ for the 29 sites averaged in North China during December 9-31. The Wangdu site is highlighted as a diamond symbol in (a) and (b).

The discrepancy between modeled and observed aerosol total Fe could be due to the model uncertainties of mineral dust aerosols caused by geographical variation of aerodynamic roughness

length, smooth roughness length and soil texture, the feedback between saltation process and friction speed, and the sandblasting efficiency[56] as well as anthropogenic dust source.[37] In addition, the anthropogenic Fe emissions could be a factor of 3-4 higher if an upper limit of anthropogenic Fe emission factor is used.[35] The aerosol Fe solubility is also uncertain. The solubility of Fe ranged from 0.05% to 1% with an average of 0.45% in total suspended particulates (TSP) collected in Dunhuang, China that is heavily affected by sandstorm from Kumtag Desert and Taklamakan Desert.[57, 58] In addition, the soluble fraction of anthropogenic Fe could vary from 0.06%-81%.[38,39] The solubility of aerosol Fe could change during long-range transport in the atmosphere.[39,40] Considering the larger uncertainties of aerosol total Fe and its solubility, it is challenging for the model to reproduce observations, and our model results seem reasonable (Fig. 2 and Table S2).

3.2 Contribution of aerosol Fe(III) photochemistry to Cl_2 production

In the base run (RUN_{Base}) without the aerosol Fe(III)-induced photolytic Cl_2 source, Cl_2 mixing ratios are generally below 1 ppt in surface air in the North China domain during the study period (Fig. 3a). This is consistent with previous modeling studies showing low Cl_2 abundance in China and around the world with the up-to-date gas-phase and multiphase Cl_2 formation mechanisms.[4,9,10,17,19] Reaction of OH with chloride on aerosols makes the largest contribution (50%) to Cl_2 production in surface air in North China in RUN_{Base}, followed by reactions of HOCl (27%), $ClNO_2$ (11%), and $ClNO_3$ (11%) with chloride on aerosols (Fig. 3b). The gas-phase mechanisms ($ClNO_3$ + Cl, ClO + ClO, and ClOO + Cl reactions) account for only 0.02% of Cl_2

production. $ClNO_2$ is the dominant reactive chlorine species in the atmospheric boundary layer while $ClNO_3$ becomes dominant in the upper troposphere (Fig. 3c). High $ClNO_2$ in the atmospheric boundary layer is due to uptake of N_2O_5 by chloride-containing aerosols while high $ClNO_3$ (from $ClO + NO_2$ reaction) in the upper troposphere is related to stratospheric transport and slow hydrolysis.[10]

After implementing the Fe(III)-induced photolytic Cl_2 formation mechanism into the model (RUN_{Fe}), Cl_2 mixing ratios increase by an order of magnitude in surface air in North China (Fig. 3d). The average surface air Cl_2 mixing ratio in North China increases from 0.5 ppt in RUN_{Base} to 5.0 ppt in RUN_{Fe}. Large Cl_2 enhancement is found in the regions where aerosol iron and chloride abundances are high (Figs. 1 and 2). On average, the Fe(III)-induced photolytic Cl_2 formation mechanism accounts for 91% of Cl_2 production in surface air in North China during the study period, followed by reactions of HOCl (4%), OH (3%), $ClNO_3$ (1%), and $ClNO_2$ (1%) with chloride on aerosols (Fig. 3e). The Fe(III)-induced photolytic Cl_2 formation mechanism is most efficient in the boundary layer where aerosol iron and chloride abundances are the highest due to emissions at the ground level (Fig. 3f). The large enhancement of Cl_2 in RUN_{Fe} not only occurs in the surface air, but also extends higher up in the atmospheric boundary layer (Fig. 3f). Measurements of Cl_2 and aerosol iron and chloride at different altitudes (e.g. using aircraft) are needed in the future to evaluate the vertical impacts of the Fe(III)-induced Cl_2 formation mechanism.

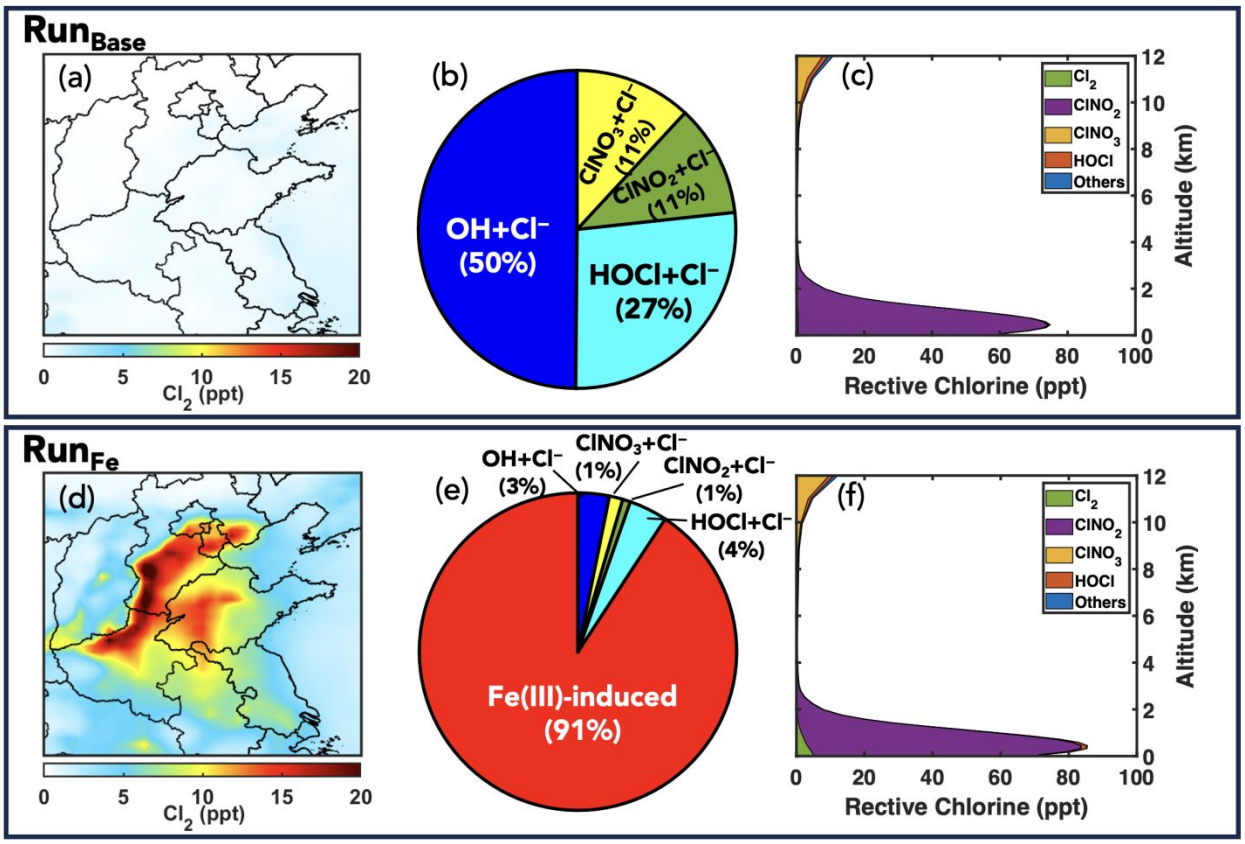

Figure 3. The average surface air Cl_2 mixing ratios (a, d), the percentage of surface air Cl_2 produced through different pathways (b, e), and the vertical distribution of reactive chlorine species (c, f) during the study period. The upper panels (a, b, c) are for RUN_{Base} and the lower panels (d, e, f) are for RUN_{Fe}. The "Others" reactive chlorine species in the right panels include Cl, ClO, ClOO, OClO, Cl_2O_2, BrCl and ICl.

3.3 Model comparison with observations at the Wangdu site

During the field campaign at the Wangdu site (Fig. 1a) in North China from December 9-31, 2017, the observed Cl_2 mixing ratio ranged from below detection limit (3 ppt) to 295 ppt, with an average of 48±51 (1σ) ppt during daytime and 28±35 (1σ) ppt at night (Figs. 4e and 5). The

observed Cl_2 generally showed a noontime peak (Fig. 5), suggesting significant photolytic Cl_2 production. In RUN_{Base}, modeled versus observed Cl_2 is only 1/83 during daytime and 1/96 at night on average during the field campaign at Wangdu (Fig. 5). This is consistent with previous modeling studies showing that traditional gas-phase and multiphase Cl_2 formation mechanisms significantly underestimate Cl_2 production in China and United States.[4,9,10,17] In comparison, in RUN_{Fe}, modeled versus observed Cl_2 is on average 1/3 during daytime and 1/2 at night, showing model's ability to simulate the magnitude of observed Cl_2 but discrepancy still exists, especially during daytime (Figs. 4e and 5). In RUN_{Fe}, Cl_2 increased after sunrise due to Fe(III)-induced aerosol photochemistry and reached about 25 ppt at noon. As shown in Figure 3e, most of the Cl_2 is produced from Fe(III)-induced aerosol photochemistry during daytime. This strong daytime Cl_2 source from Fe(III)-induced aerosol photochemistry maintains Cl_2 levels of 10-30 ppt during daytime when Cl_2 is otherwise rapidly photolyzed (lifetime of 17 min around noon). It also improves the model's performance for Cl_2 at night when rapid photolytic Cl_2 loss disappears after sunset (Fig. 5).

The NO_2 photolysis frequency, aerosol chloride, aerosol Fe(III), and aerosol surface area concentrations are important factors for Fe(III)-induced photolytic Cl_2 production. At the Wangdu site during daytime, the model (RUN_{Fe}) can basically reproduce the diurnal pattern of observed j_{NO2}, with 17% model overestimation (Fig. 4a). The model overestimates observed aerosol chloride and aerosol total Fe mass concentrations by 63% and 29% on average during daytime, respectively (Figs. 4c-d). The model overestimates the aerosol surface area concentration by a factor of 3 on

average during daytime (Fig. 4b). The model overestimation of aerosol surface area concentration could be due to model overestimation of aerosol growth factor calculated using the aerosol water content from the ISORROPIA thermodynamic module. The overestimation of aerosol water content could lead to underestimation of chloride and Fe(III) molar concentrations, and subsequently inefficient Cl_2 production from Fe(III)-induced aerosol photochemistry. In particular, the model (RUN_{Fe}) overestimates observed daytime aerosol surface area concentration by a factor of 12 (12440 μm^2 cm^{-3} modeled *versus* 930 μm^2 cm^{-3} observed) on December 29, while it underestimates observed daytime Cl_2 by 84% (3.4 ppt modeled *versus* 20.8 ppt observed).

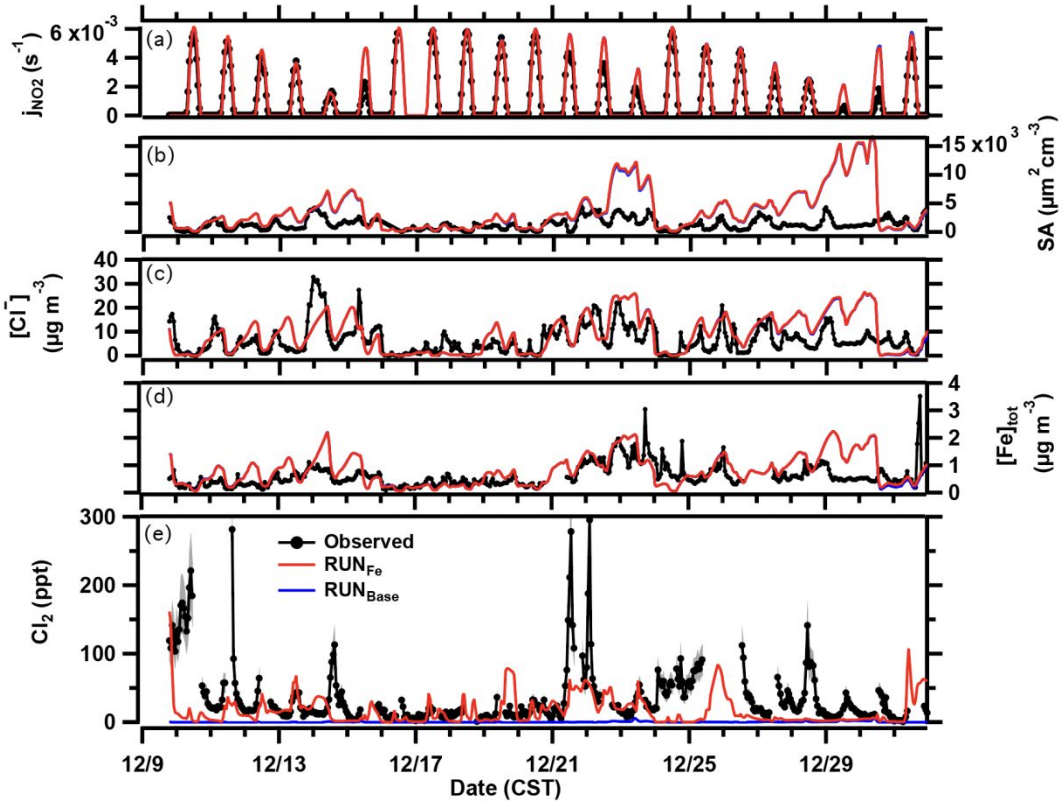

Figure 4. Comparison of modeled and observed Cl_2 as well as key factors for aerosol iron photochemistry (j_{NO2}, SA, $[Cl^-]$ and $[Fe]_{tot}$) at the Wangdu site during the study period (December 09-31, 2023). The grey shading in (e) represents measurement uncertainties of Cl_2. In (e), the linear regression R^2 value for modelled versus observed Cl_2 is 0.06 for RUN_{Fe} and 0.01 for RUN_{Base}.

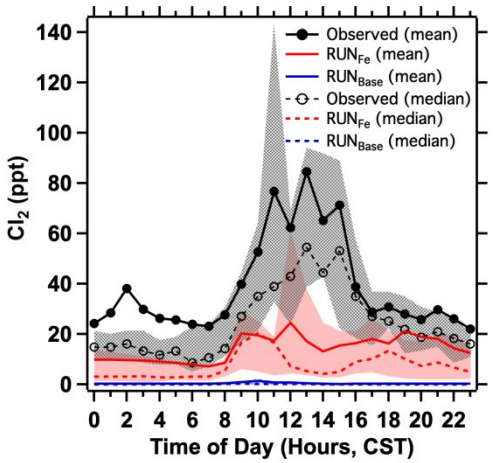

Figure 5. The diel pattern of Cl_2 observed and modeled. The mean (solid lines), median (dash lines), 25% and 75% percentiles (shadings) are shown.

Both RUN_{Base} and RUN_{Fe} can reasonably simulate the daily and diurnal variations of the air temperature, relative humidity, NO, NO_2, O_3, $PM_{2.5}$ nitrate, sulfate and ammonium concentrations at the Wangdu site (Fig. S1). However, both model runs overestimate observed NO and underestimate observed O_3 in general. On average, NO is overestimated by 78% in RUN_{Base} and 71% in RUN_{Fe}, respectively (Fig. S1c). As a result, O_3 is on average underestimated by 58% in RUN_{Base} and 51% in RUN_{Fe}, respectively (Fig. S1e). In comparison, the discrepancies between

modeled (33±14 ppt in RUN_{Base} and 35±15 ppt in RUN_{Fe}) and observed NO_2 (30±14 ppt) are smaller (Fig. S1d).

3.4 Impacts on atmospheric oxidative capacity and air quality

The Cl radical concentration is typically on the order of 10^2 cm^{-3} in North China in RUN_{Base}, but increases to 10^3 cm^{-3} in RUN_{Fe} due to the increase of Cl_2 (Fig. 6). This is consistent with a previous regional modeling (CMAQ) study showing 10^3-10^4 cm^{-3} Cl concentration in North China during summer with daytime Cl_2 on the order of tens to hundreds of ppt. In RUN_{Base}, $ClNO_2$ photolysis accounts for most (83%) of Cl radicals in North China, followed by Cl_2 photolysis (11%), HCl+OH reaction (4%), and HOCl photolysis (2%). In contrast, in RUN_{Fe}, Cl_2 photolysis becomes the dominant (65%) Cl source in North China, followed by $ClNO_2$ photolysis (32%), HCl+OH reaction (2%), and HOCl photolysis (1%). Cl_2 photolysis acting as the dominant source of Cl radicals has been observed in previous field studies in China where tens to hundreds of ppt daytime Cl_2 was observed.[15-17] As a result of VOCs oxidation by Cl, the OH radical concentration increases by 9% on average in the North China domain during the study period, and typically 20-40% in the central part of the domain (Fig. 6). Oxidation of VOCs by Cl radicals produces peroxy radicals (RO_2), which further produces HO_2 and OH radicals in the presence of NO_x.[1,2,14,15] The slight decrease of OH in the northern part of the domain is a result of reactive chlorine chemistry converting OH/HO_2 to Cl/ClO.[1] The enhancement of Cl and OH abundances together increase the

reactivities of ethane, propane, methanol, ethanol, ≥C_3 alkenes, and toluene by 60%, 50%, 35%, 19%, 7%, and 6% on average, respectively, in surface air in North China.

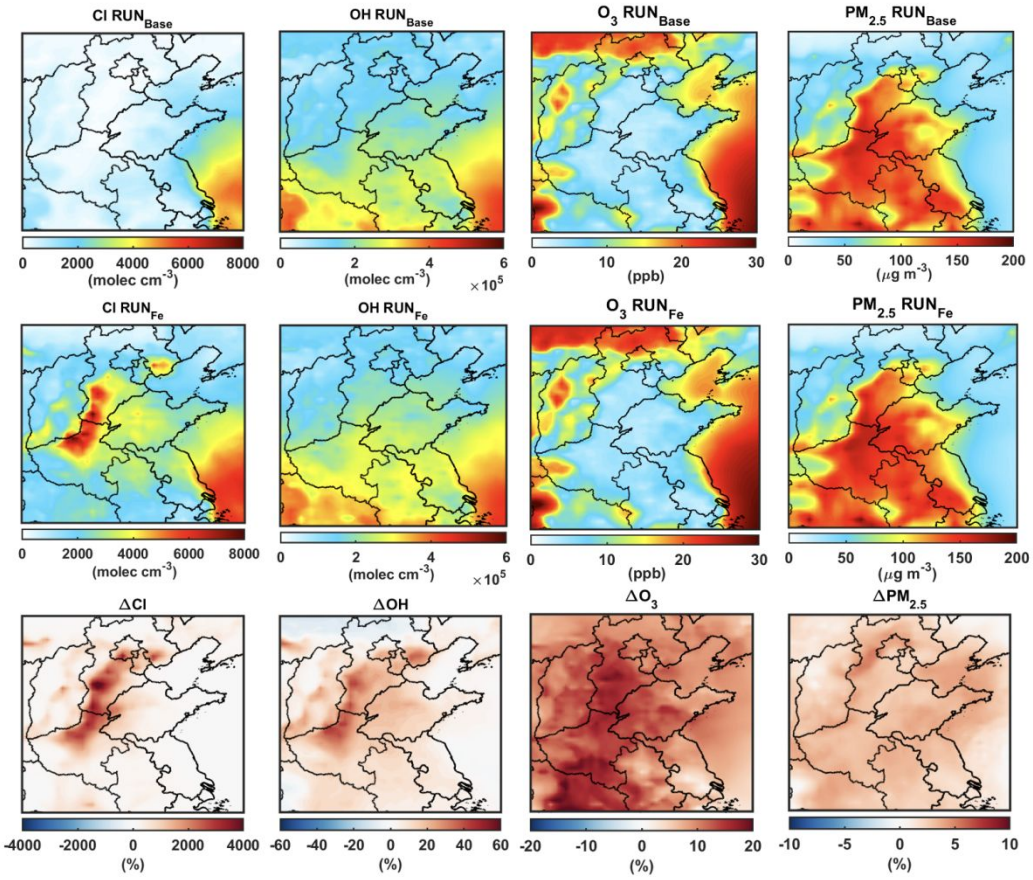

Figure 6. Impacts of aerosol Fe(III)-induced photolytic Cl_2 source on chlorine radical (Cl), hydroxyl radical (OH), ozone (O_3), and fine particulate matter ($PM_{2.5}$) concentrations in surface air during the study period. Concentrations of species in both RUN_{Base} and RUN_{Fe} are shown. The percentage differences are calculated as $(RUN_{Fe} - RUN_{Base})/RUN_{Base}$.

The production of peroxy radicals from oxidation of VOCs by Cl radicals can contribute to O_3 formation in the NO_x polluted environment.[1,59] On the other hand, Cl reacting with O_3 and ClO reacting with NO_2 can initiate the removal of O_3 and NO_x,[2,10] and the OH produced from Cl oxidation can also contribute to the removal of NO_x through the NO_2 + OH reaction. In wintertime North China with high VOCs and low O_3, the fraction of Cl reacting with O_3 is generally lower than 20% (Fig. S6) so that Cl reacts with VOCs to generate O_3. With the Fe(III)-induced photolytic Cl_2 added to the model, surface air O_3 generally increases by <20% (on average 10%) in North China (Fig. 6), while NO_x generally decreases by <5% (on average 3%) (Fig. S2). This is consistent with a previous regional modeling study showing <10% increase of O_3 in North China during summer with the modeled daytime Cl_2 increasing from near zero to hundreds of ppt.[4]

The implementation of the Fe(III)-induced photolytic Cl_2 source in the model results in an increase of surface air $PM_{2.5}$ concentration in North China by only 3% on average (Fig. 6), mainly caused by the increase (10% on average) of aerosol nitrate concentration (up to 4 μg m^{-3}) (Fig. S3-S4). The increase of nitrate is mainly due to the enhanced nitrate production rate from NO_2 + OH and N_2O_5 hydrolysis in RUN_{Fe}. The increase of nitrate results in an increase of ammonium by 6% on average in North China (up to 1 μg m^{-3}) through the formation of NH_4NO_3 in the ISORROPIA thermodynamic system (Fig. S3-S4). Sulfate shows negligible (<0.3 μg m^{-3}) change in RUN_{Fe} compared to RUN_{Base} (Fig. S3-S4). The impact of the Fe(III)-induced photolytic Cl_2 on SOA was not investigated in this study, as our model used a fixed-yield approach for SOA formation (default setup) and did not include SOA formation from oxidation of VOCs by Cl radicals, as explained in

Section 2.[2,47,48] This should be investigated in the future, as the Fe(III)-induced photolytic Cl_2 has significantly enhanced the Cl radical concentrations and subsequent VOCs oxidation.

3.5 Uncertainties and Implications

The uncertainties of aerosol Fe(III) and chloride as well as aerosol surface area concentrations and sunlight intensity will affect the amount of Cl_2 produced via aerosol iron photochemistry, as shown in previous sections. It is challenging to quantify these uncertainties due to sparse observational data. We have used aerosol soluble iron concentration measurements at two sites in North China as observational constraints, with model underestimation of 31% in Beijing and model overestimation of 69% in Handan (Table S2). Measurements at more sites will be needed in the future for better constraints. The Fe(III) fraction of aerosol soluble iron was not measured in North China, but we have used the value obtained from Asian continental outflow daytime aerosol samples, with an uncertainty of 12%.[33] Considering uncertainties of both aerosol soluble iron concentration and Fe(III) fraction, we estimate $0.5[Fe^{3+}]$ and $1.6[Fe^{3+}]$ in the current model run as the lower limit and upper limit, respectively. Aerosol chloride concentration is overestimated by 50% on average for the 29 sites in North China. Thus, we estimate $0.7[Cl^-]$ and $[Cl^-]$ in the current model run as the lower limit and upper limit, respectively. Then, considering uncertainties of both $[Fe^{3+}]$ and $[Cl^-]$, the lower limit and upper limit of Fe(III)-induced Cl_2 production rate are estimated to be 35% and 160% of the current model results, respectively. Aerosol surface area concentration could be highly uncertain and it is associated with the model's

performance of aerosol thermodynamics, which also affects aerosol acidity and solute concentrations. The aerosol surface area concentration is overestimated by a factor of 3 at the Wangdu site during daytime, but measurements at more sites are needed to better assess the model performance. j_{NO2} is overestimated by 17% at the Wangdu site. Photolysis of NO_2 occurs in the solar radiation spectrum[77] of 290-430 nm while photolysis of Fe(III)-Cl (mostly $FeCl_2^+$) is active in the range of 400-530 nm. [74] Thus, field measurements of actinic flux over 400-530 nm in the future will be useful to constrain the Fe(III)-induced Cl_2 formation mechanism.

Our parameterization of Fe(III)-induced photolytic Cl_2 formation mechanism is simplified and does not consider suppression effects of sulfate and organics. It has been shown in laboratory experiments that sulfate and organics inhibit Fe(III)-induced photolytic Cl_2 production.[21] Sulfate can react with Fe(II) to form $FeSO_4$ complex, interrupting the regeneration of Fe(II) to Fe(III).[21,60,74,75] Sulfate can also react with Fe(III) to form $FeSO_4^+$ and $Fe(SO_4)_2^-$ complexes, reducing the availability of Fe(III) to form Fe(III)-Cl complexes. [21,60,74,75] The organics present in aerosols such as oxalic acid and catechol could form stable complexes with Fe(III) to diminish the Fe(III)-Cl complexation.[21,78,79] Organics can also react with $OH_{(aq)}$, $Cl_{(aq)}$, and Cl_2^- radicals within aerosols to intervene Cl_2 formation.[80,81] In addition, previous laboratory experiments showed that black iron-catechol complex could form within aerosols and intervene photolysis of Fe(III)-Cl complexes.[21] Further investigation is necessary to quantify the suppression effects of sulfate and organics on Fe(III)-induced photolytic Cl_2 formation.

Aerosol acidity can affect the solubility and speciation of Fe(III). The solubility of Fe(III) increases as pH decreases.[61] Both Fe(III)-Cl and Fe(III)-hydroxy complexes can produce Cl_2 (*R*1-*R*11), but Fe(III)-Cl complexes are more photoactive in generating aqueous phase Cl radicals while Fe(III)-hydroxy complexes produce aqueous phase Cl radicals indirectly through generating aqueous phase OH radicals.[20,21,23] At lower aerosol pH, especially < 4.5, the Fe(III)-Cl complexes are expected to be the dominant form of Fe(III).[20,74] Formation of $FeSO_4^+$ complex is also facilitated at such low aerosol pH.[74] However, at aerosol pH > 4.5, the fraction of Fe(III)-hydroxy complexes increases while the fraction of Fe(III)-Cl complexes decreases rapidly.[20,74] The aerosol pH was estimated in the model to range from 2.1 to 6.3 in surface air of the study domain, with an average of 4.3±1.0 (Fig. S5). Based on the soluble aerosol Fe as well as single particle measurements in North China during part of the study period (December 21-31, 2017), Zhu et al.[41] suggested that the Fe-containing aerosols were mainly smaller than 1 μm and have undergone acidic processes. Aerosol particle acidity could increase with decreasing particle size such that pH of smaller particles could be lower than the bulk particle pH.[62, 63] Since the actual pH of Fe-containing aerosols and the effect of pH on the Fe(III)-induced Cl_2 production rate have not been quantified, we did not include the pH effect on Fe(III)-induced Cl_2 production in this study. This should be further quantified in laboratory experiments in the future.

Recently, Peng et al.[15] proposed that aerosol nitrate photolysis could initiate Cl_2 production at coastal Hong Kong when aerosol pH is < 3.3 (*R*12-*R*15, *R*5-*R*11). The generation of $OH_{(aq)}$ from

nitrate photolysis in aerosols is accelerated by acidity,[15,76] and the Cl_2 production initiated by $OH_{(aq)}$ is also acidity dependent (*R*5-*R*11).

$$NO_3^- + h\nu \rightarrow O^- + NO_{2(aq)} \quad (yield \sim 0.01) \qquad (R12a)$$

$$\rightarrow O_{(aq)} + NO_2^- \quad (yield \sim 0.001) \qquad (R12b)$$

$$O^- + H^+ \rightleftharpoons OH_{(aq)} \qquad (R13)$$

$$NO_2^- + H^+ \rightleftharpoons HONO_{(aq)} \qquad (R14)$$

$$HONO_{(aq)} + h\nu \rightarrow NO_{(aq)} + OH_{(aq)} \qquad (R15)$$

The aerosol pH calculated by the ISORROPIA thermodynamic module in GEOS-Chem was on average 4.3±1.0 in the study domain (Fig. S5) due to high ammonia (NH_3) emissions from agriculture.[64,65] Nevertheless, as discussed previously, aerosol pH could be lower in Fe-containing aerosols.[41] The Cl_2 production mechanism of nitrate photolysis was not included in this study.

In addition, uptake of O_3 by aerosols was previously proposed to explain the high Cl_2 observed in North China.[4] However, the uptake coefficient of O_3 (γ_{O3}) is highly uncertain. From previous laboratory experiments, γ_{O3} was < 1×10^{-4} for deliquesced NaCl aerosols,[66] but could increase to 3×10^{-2} when NaCl was mixed with $FeCl_3$.[67] Recent experiments by Faxon et al.[68] showed that γ_{O3} could reach 1×10^{-3} on deliquesced pure NH_4Cl aerosols but decrease to 1×10^{-5} in the presence of SOA. Qiu et al.[4] used a high γ_{O3} (1×10^{-3}) during daytime and a low γ_{O3} (1×10^{-5}) at night in their CMAQ chemical transport model to simulate the high daytime Cl_2 and low nighttime Cl_2 observed in Wangdu in North China during summer. However, it is unclear why γ_{O3} would differ by two

orders of magnitude between daytime and nighttime. Recently, Chen et al.[17] used a box model to simulate Cl_2 formation at a suburban site in East China and found that using $\gamma_{O3} = 1\times10^{-5}$ would reproduce the observed daytime Cl_2 of about 10 ppt but overestimate nighttime Cl_2 by a factor of 6. Using $\gamma_{O3} = 1\times10^{-3}$, their model overestimated observed Cl_2 by almost two orders of magnitude. Due to the large uncertainties in γ_{O3} and that it would either over-predict nighttime Cl_2 production or under-predict daytime Cl_2 production if the same γ_{O3} is used throughout the day, the O_3 uptake mechanism was not included in our model.

In summary, the Fe(III)-induced photolytic Cl_2 formation mechanism was implemented into a chemical transport model, and its impacts on atmospheric Cl_2 budget, oxidative capacity, and air quality in wintertime North China were examined. The model generally shows good performance in simulating the average aerosol iron and chloride concentrations observed at 29 sites in the study domain. The Fe(III)-induced photolytic Cl_2 formation mechanism, accounting for more than 90% of Cl_2 production, causes an order of magnitude increases in Cl_2 in surface air in North China. With the Fe(III)-induced photolytic Cl_2 formation mechanism, the model better simulates Cl_2 observed at the Wangdu sampling site, but still underestimates daytime values a factor of 3 on average. The Fe(III)-induced photolytic Cl_2 formation mechanism is uncertain, and further investigations are needed to quantify the effects of aerosol acidity, sulfate, and organics. More field measurements of aerosol Fe(III) and chloride concentrations as well as aerosol surface area concentration in different environments and at different altitudes are also needed to better constrain

this Cl_2 formation mechanism. This study offers new insight into the high daytime Cl_2 production in polluted environment.

ASSOCIATED CONTENT

Supporting Information. Parameterization of aerosol Fe(III)-induced photolytic Cl_2 production (Text S1). The updated Cl_2 formation mechanisms in GEOS-Chem (Table S1). The comparison between modeled and observed aerosol iron solubility at the Beijing and Handan sites in North China (Table S2). Comparison of modeled and observed meteorological parameters and chemical species at the Wangdu site during the study period (Figure S1). The change of NO_x after adding aerosol Fe(III)-induced photolytic Cl_2 source (Figure S2). The change of aerosol nitrate, sulfate, and ammonium after adding aerosol Fe(III)-induced photolytic Cl_2 source (Figure S3). Comparison of modeled and observed aerosol nitrate, sulfate and ammonium concentrations for the "2+26" cities in North China (Figure S4). The fine-mode aerosol pH in surface air of the study domain (Figure S5). The fraction of Cl reacting with O_3 in surface air of the study domain (Figure S6).

AUTHOR INFORMATION

Corresponding Author

* Qianjie Chen - Department of Civil and Environmental Engineering, Hong Kong Polytechnic University, Hong Kong SAR, China; https://orcid.org/0000-0003-4737-5179; Email: qianjie.chen@polyu.edu.hk

* Tao Wang - Department of Civil and Environmental Engineering, Hong Kong Polytechnic University, Hong Kong SAR, China; https://orcid.org/0000-0002-4765-9377; Email: tao.wang@polyu.edu.hk

Present Addresses

‡ Department of Ambient Air Quality Monitoring, China National Environmental Monitoring Center, Beijing, 100012, China.

♀ Hangzhou PuYu Technology Development Co., Ltd, Hangzhou, Zhejiang, 311300, China.

† Institute for Atmospheric and Earth System Research/Physics, University of Helsinki, Helsinki 00014, Finland

Author Contributions

QC conceived this modelling study. QC and TW designed the research. XW and XF provided anthropogenic chlorine emissions in China. XW, BA, and QC led model development of reactive chlorine chemistry and aerosol iron simulation. QC implemented aerosol iron-induced Cl_2 formation mechanism in GEOS-Chem. TW designed the halogen research at Wangdu. XP, WW and MX conducted Cl_2 measurements at Wangdu. JG provided aerosol iron, chlorine, nitrate,

sulfate, and ammonium data for the "2+26" cities in North China. JC and YM planned and organized the overall field campaign at Wangdu. PL performed particulate matter measurements at Wangdu. XL and YT contributed to data analysis and manuscript revision. QC analyzed the data and wrote the manuscript with contributions from all co-authors. All authors have given approval to the final version of the manuscript.

Funding Sources

This study is supported by the Hong Kong Research Grants Council (Grant No. 15219722, 15223221, 15207421, and T24-504/17-N) and the National Natural Science Foundation of China (Grant No. 42205115). XF was supported by National Natural Science Foundation of China (Grant No. 22206106) and Municipal Science and Technology Innovation Commission of Shenzhen (JCYJ20220530143007016). BA was supported by the National Science Foundation Grant AGS 2109323.

Notes

The authors declare no competing financial interest.

ACKNOWLEDGMENT

This study is supported by the Hong Kong Research Grants Council (Grant No. 15219722, 15223221, 15207421, and T24-504/17-N) and the National Natural Science Foundation of China

(Grant No. 42205115). QC acknowledges Dr. Cornelius Zetzsch for helpful information on the aerosol iron photochemistry experiments conducted in Wittmer et al.[20].

REFERENCES

1. Simpson, W. R.; Brown, S. S.; Saiz-Lopez, A.; Thornton, J. A.; von Glasow, R. Tropospheric Halogen Chemistry: Sources, Cycling, and Impacts. *Chemical Reviews* **2015,** *115* (10), 4035-4062.

2. Wang, X.; Jacob, D. J.; Fu, X.; Wang, T.; Le Breton, M.; Hallquist, M.; Liu, Z.; McDuffie, E. E.; Liao, H. Effects of Anthropogenic Chlorine on PM 2.5 and Ozone Air Quality in China. *Environmental Science & Technology* **2020,** *54* (16), 9908-9916.

3. Li, Q.; Fu, X.; Peng, X.; Wang, W.; Badia, A.; Fernandez, R. P.; Cuevas, C. A.; Mu, Y.; Chen, J.; Jimenez, J. L.; Wang, T.; Saiz-Lopez, A. Halogens Enhance Haze Pollution in China. *Environmental Science & Technology* **2021,** *55* (20), 13625-13637.

4. Qiu, X.; Ying, Q.; Wang, S.; Duan, L.; Wang, Y.; Lu, K.; Wang, P.; Xing, J.; Zheng, M.; Zhao, M.; Zheng, H.; Zhang, Y.; Hao, J. Significant Impact of Heterogeneous Reactions of Reactive Chlorine Species on Summertime Atmospheric Ozone and Free-radical Formation in North China. *Science of the Total Environment* **2019,** *693*, 133580.

5. Wang, D. S.; Hildebrandt Ruiz, L. Secondary Organic Aerosol from Chlorine-Initiated Oxidation of Isoprene. *Atmospheric Chemistry and Physics* **2017,** *17* (22), 13491-13508.

6. Strode, S. A.; Wang, J.; Manyin, M.; Duncan, B.; Hossaini, R.; Keller, C. A.; Michel, S. E.; White, J. W. C. Strong Sensitivity of the Isotopic Composition of Methane to the Plausible Range of Tropospheric Chlorine. *Atmospheric Chemistry and Physics* **2020,** *20* (14), 8405-8419.

7. Bock, M.; Schmitt, J.; Beck, J.; Seth, B.; Chappellaz, J.; Fischer, H. Glacial/interglacial Wetland, Biomass Burning, and Geologic Methane Emissions Constrained by Dual Stable Isotopic CH_4 Ice Core Records. *Proceedings of the National Academy of Sciences of the United States of America* **2017,** *114* (29), 5778-5786.

8. Chen, Q.; Sherwen, T.; Evans, M.; Alexander, B. DMS Oxidation and Sulfur Aerosol Formation in the Marine Troposphere: A Focus on Reactive Halogen and Multiphase Chemistry. *Atmospheric Chemistry and Physics* **2018,** *18* (18), 13617-13637.

9. Wang, X.; Jacob, D. J.; Downs, W.; Zhai, S.; Zhu, L.; Shah, V.; Holmes, C. D.; Sherwen, T.; Alexander, B.; Evans, M. J.; Eastham, S. D.; Neuman, J. A.; Veres, P. R.; Koenig, T. K.; Volkamer, R.; Huey, L. G.; Bannan, T. J.; Percival, C. J.; Lee, B. H.; Thornton, J. A. Global Tropospheric Halogen (Cl, Br, I) Chemistry and its Impact on Oxidants. *Atmospheric Chemistry and Physics* **2021,** *21* (18), 13973-13996.

10. Wang, X.; Jacob, D. J.; Eastham, S. D.; Sulprizio, M. P.; Zhu, L.; Chen, Q.; Alexander, B.; Sherwen, T.; Evans, M. J.; Lee, B. H.; Haskins, J. D.; Lopez-Hilfiker, F. D.; Thornton, J. A.; Huey, G. L.; Liao, H. The Role of Chlorine in Global Tropospheric Chemistry. *Atmospheric Chemistry and Physics* **2019,** *19* (6), 3981-4003.

11. Osthoff, H. D.; Roberts, J. M.; Ravishankara, A. R.; Williams, E. J.; Lerner, B. M.; Sommariva, R.; Bates, T. S.; Coffman, D.; Quinn, P. K.; Dibb, J. E.; Stark, H.; Burkholder, J. B.; Talukdar, R. K.; Meagher, J.; Fehsenfeld, F. C.; Brown, S. S. High Levels of Nitryl Chloride in the Polluted Subtropical Marine Boundary Layer. *Nature Geoscience* **2008,** *1* (5), 324-328.

12. Thornton, J. A.; Kercher, J. P.; Riedel, T. P.; Wagner, N. L.; Cozic, J.; Holloway, J. S.; Dubé, W. P.; Wolfe, G. M.; Quinn, P. K.; Middlebrook, A. M.; Alexander, B.; Brown, S. S. A Large Atomic Chlorine Source Inferred from Mid-continental Reactive Nitrogen Chemistry. *Nature* **2010,** *464* (7286), 271-274.

13. McNamara, S. M.; Kolesar, K. R.; Wang, S. Y.; Kirpes, R. M.; May, N. W.; Gunsch, M. J.; Cook, R. D.; Fuentes, J. D.; Hornbrook, R. S.; Apel, E. C.; China, S.; Laskin, A.; Pratt, K. A. Observation of Road Salt Aerosol Driving Inland Wintertime Atmospheric Chlorine Chemistry. *ACS Central Science* **2020,** *6* (5), 684-694.

14. Peng, X.; Wang, W.; Xia, M.; Chen, H.; Ravishankara, A. R.; Li, Q.; Saiz-Lopez, A.; Liu, P.; Zhang, F.; Zhang, C. L.; Xue, L.; Wang, X.; George, C.; Wang, J.; Mu, Y.; Chen, J.; Wang, T. An Unexpected Large Continental Source of Reactive Bromine and Chlorine with Significant Impact on Wintertime Air Quality. *National Science Review* **2021,** *8* (7), nwaa304.

15. Peng, X.; Wang, T.; Wang, W.; Ravishankara, A. R.; George, C.; Xia, M.; Cai, M.; Li, Q.; Salvador, C. M.; Lau, C.; Lyu, X.; Poon, C. N.; Mellouki, A.; Mu, Y.; Hallquist, M.; Saiz-

Lopez, A.; Guo, H.; Herrmann, H.; Yu, C.; Dai, J.; Wang, Y.; Wang, X.; Yu, A.; Leung, K.; Lee, S.; Chen, J. Photodissociation of Particulate Nitrate as a Source of Daytime Tropospheric Cl_2. *Nature Communications* **2022,** *13*, 939.

16. Liu, X.; Qu, H.; Huey, L. G.; Wang, Y.; Sjostedt, S.; Zeng, L.; Lu, K.; Wu, Y.; Ho, M.; Shao, M.; Zhu, T.; Zhang, Y. High Levels of Daytime Molecular Chlorine and Nitryl Chloride at a Rural Site on the North China Plain. *Environmental Science & Technology* **2017,** *51* (17), 9588-9595.

17. Chen, Q.; Xia, M.; Peng, X.; Yu, C.; Sun, P.; Li, Y.; Liu, Y.; Xu, Z. N.; Xu, Z.; Wu, R.; Nie, W.; Ding, A.; Zhao, Y.; Wang, T. Large Daytime Molecular Chlorine Missing Source at a Suburban Site in East China. *Journal of Geophysical Research-Atmospheres* **2022,** *127*, e2021JD035796.

18. Xia, M.; Peng, X.; Wang, W.; Yu, C.; Sun, P.; Li, Y.; Liu, Y.; Xu, Z. N.; Wang, Z.; Xu, Z.; Nie, W.; Ding, A.; Wang, T. Significant Production of $ClNO_2$ and Possible Source of Cl_2 from N_2O_5 Uptake at a Suburban Site in Eastern China. *Atmospheric Chemistry and Physics* **2020,** *20* (10), 6147-6158.

19. Le Breton, M.; Bannan, T. J.; Shallcross, D. E.; Khan, M. A.; Evans, M. J.; Lee, J.; Lidster, R.; Andrews, S.; Carpenter, L. J.; Schmidt, J.; Jacob, D.; Harris, N. R. P.; Bauguitte, S.; Gallagher, M.; Bacak, A.; Leather, K. E.; Percival, C. J. Enhanced Ozone Loss by Active Inorganic Bromine Chemistry in the Tropical Troposphere. *Atmospheric Environment* **2017,** *155*, 21-28.

20. Wittmer, J.; Bleicher, S.; Ofner, J.; Zetzsch, C. Iron(III)-induced Activation of Chloride from Artificial Sea-salt Aerosol. *Environmental Chemistry* **2015,** *12* (4), 461-475.

21. Wittmer, J.; Bleicher, S.; Zetzsch, C. Iron(III)-Induced Activation of Chloride and Bromide from Modeled Salt Pans. *Journal of Physical Chemistry A* **2015,** *119* (19), 4373-4385.

22. van-Herpen, M. M. J. W.; Li, Q.; Saiz-Lopez, A.; Liisberg, J. B.; Röckmann, T.; Cuevas, C. A.; Fernandez, R. P.; Mak, J. E.; Mahowald, N. M.; Hess, P.; Meidan, D.; Stuut, J.-B. W.; Johnson, M. S. Photocatalytic Chlorine Atom Production on Mineral Dust–sea Spray Aerosols over the North Atlantic. *Proceedings of the National Academy of Sciences* **2023,** *120* (31), e2303974120.

23. Lim, M.; Chiang, K.; Amal, R. Photochemical Synthesis of Chlorine Gas from Iron(III) and Chloride Solution. *Journal of Photochemistry and Photobiology a-Chemistry* **2006,** *183* (1-2), 126-132.

24. Oeste, F. D.; de Richter, R.; Ming, T. Z.; Caillol, S. Climate Engineering by Mimicking Natural Dust Climate Control: the Iron Salt Aerosol Method. *Earth System Dynamics* **2017,** *8* (1), 1-54.

25. Ming, T.; de Richter, R.; Oeste, F. D.; Tulip, R.; Caillol, S. A Nature-based Negative Emissions Technology able to Remove Atmospheric Methane and other Greenhouse Gases. *Atmospheric Pollution Research* **2021,** *12* (5), 101035.

26. Schmidt, J. A.; Jacob, D. J.; Horowitz, H. M.; Hu, L.; Sherwen, T.; Evans, M. J.; Liang, Q.; Suleiman, R. M.; Oram, D. E.; Le Breton, M.; Percival, C. J.; Wang, S.; Dix, B.; Volkamer,

R. Modeling the Observed Tropospheric BrO Background: Importance of Multiphase Chemistry and Implications for Ozone, OH, and Mercury. *Journal of Geophysical Research-Atmospheres* **2016,** *121* (19), 11819-11835.

27. Sherwen, T.; Schmidt, J. A.; Evans, M. J.; Carpenter, L. J.; Grossmann, K.; Eastham, S. D.; Jacob, D. J.; Dix, B.; Koenig, T. K.; Sinreich, R.; Ortega, I.; Volkamer, R.; Saiz-Lopez, A.; Prados-Roman, C.; Mahajan, A. S.; Ordóñez, C. Global Impacts of Tropospheric Halogens (Cl, Br, I) on Oxidants and Composition in GEOS-Chem. *Atmospheric Chemistry and Physics* **2016,** *16* (18), 12239-12271.

28. Chen, Q.; Schmidt, J. A.; Shah, V.; Jaeglé, L.; Sherwen, T.; Alexander, B. Sulfate Production by Reactive Bromine: Implications for the Global Sulfur and Reactive Bromine Budgets. *Geophysical Research Letters* **2017,** *44* (13), 7069-7078.

29. Fountoukis, C.; Nenes, A. ISORROPIA II: A Computationally Efficient Thermodynamic Equilibrium Model for K^+–Ca^{2+}–Mg^{2+}–NH_4^+–Na^+–SO_4^{2-}–NO_3^-–Cl^-–H_2O Aerosols. *Atmospheric Chemistry and Physics* **2007,** *7* (17), 4639-4659.

30. Fu, X.; Wang, T.; Wang, S.; Zhang, L.; Cai, S.; Xing, J.; Hao, J. Anthropogenic Emissions of Hydrogen Chloride and Fine Particulate Chloride in China. *Environmental Science & Technology* **2018,** *52* (3), 1644-1654.

31. Zheng, B.; Tong, D.; Li, M.; Liu, F.; Hong, C.; Geng, G.; Li, H.; Li, X.; Peng, L.; Qi, J.; Yan, L.; Zhang, Y.; Zhao, H.; Zheng, Y.; He, K.; Zhang, Q. Trends in China's Anthropogenic

Emissions since 2010 as the Consequence of Clean Air Actions. *Atmospheric Chemistry and Physics* **2018,** *18* (19), 14095-14111.

32. Yin, L.; Du, P.; Zhang, M.; Liu, M.; Xu, T.; Song, Y. Estimation of Emissions from Biomass Burning in China (2003-2017) based on MODIS Fire Radiative Energy Data. *Biogeosciences* **2019,** *16* (7), 1629-1640.

33. Moffet, R. C.; Furutani, H.; Rödel, T. C.; Henn, T. R.; Sprau, P. O.; Laskin, A.; Uematsu, M.; Gilles, M. K. Iron Speciation and Mixing in Single Aerosol Particles from the Asian Continental Outflow. *Journal of Geophysical Research* **2012,** *117*, D07204.

34. Zhu, Y.; Li, W.; Wang, Y.; Zhang, J.; Liu, L.; Xu, L.; Xu, J.; Shi, J.; Shao, L.; Fu, P.; Zhang, D.; Shi, Z. Sources and Processes of Iron Aerosols in a Megacity in Eastern China. *Atmospheric Chemistry and Physics* **2022,** *22* (4), 2191-2202.

35. Alexander, B.; Park, R. J.; Jacob, D. J.; Gong, S. Transition Metal-catalyzed Oxidation of Atmospheric Sulfur: Global Implications for the Sulfur Budget. *Journal of Geophysical Research-Atmospheres* **2009,** *114*, D02309.

36. Shao, J.; Chen, Q.; Wang, Y.; Lu, X.; He, P.; Sun, Y.; Shah, V.; Martin, R. V.; Philip, S.; Song, S.; Zhao, Y.; Xie, Z.; Zhang, L.; Alexander, B. Heterogeneous Sulfate Aerosol Formation Mechanisms During Wintertime Chinese Haze Events: Air Quality Model Assessment Using Observations of Sulfate Oxygen Isotopes in Beijing. *Atmospheric Chemistry and Physics* **2019,** *19* (9), 6107-6123.

37. Philip, S.; Martin, R. V.; Snider, G.; Weagle, C. L.; van Donkelaar, A.; Brauer, M.; Henze, D. K.; Klimont, Z.; Venkataraman, C.; Guttikunda, S. K.; Zhang, Q. Anthropogenic Fugitive, Combustion and Industrial Dust is a Significant, Underrepresented Fine Particulate Matter Source in Global Atmospheric Models. *Environmental Research Letters* **2017,** *12*, 044018.

38. Oakes, M.; Ingall, E. D.; Lai, B.; Shafer, M. M.; Hays, M. D.; Liu, Z.; Russell, A. G.; Weber, R. J. Iron Solubility Related to Particle Sulfur Content in Source Emission and Ambient Fine Particles. *Environmental Science & Technology* **2012,** *46* (12), 6637-6644.

39. Ito, A.; Ye, Y.; Baldo, C.; Shi, Z. Ocean Fertilization by Pyrogenic Aerosol Iron. *npj Climate and Atmospheric Science* **2021,** *4* (1), 30.

40. Fu, H.; Lin, J.; Shang, G.; Dong, W.; Grassian, V. H.; Carmichael, G. R.; Li, Y.; Chen, J. Solubility of Iron from Combustion Source Particles in Acidic Media Linked to Iron Speciation. *Environmental Science & Technology* **2012,** *46* (20), 11119-11127.

41. Zhu, Y.; Li, W.; Lin, Q.; Yuan, Q.; Liu, L.; Zhang, J.; Zhang, Y.; Shao, L.; Niu, H.; Yang, S.; Shi, Z. Iron Solubility in Fine Particles Associated with Secondary Acidic Aerosols in East China. *Environmental Pollution* **2020,** *264*, 114769.

42. Schroth, A. W.; Crusius, J.; Sholkovitz, E. R.; Bostick, B. C. Iron Solubility Driven by Speciation in Dust Sources to the Ocean. *Nature Geoscience* **2009,** *2* (5), 337-340.

43. Deguillaume, L.; Leriche, M.; Desboeufs, K.; Mailhot, G.; George, C.; Chaumerliac, N. Transition Metals in Atmospheric Liquid Phases: Sources, Reactivity, and Sensitive Parameters. *Chemical Reviews* **2005,** *105* (9), 3388-3431.

44. Mao, J.; Fan, S.; Horowitz, L. W. Soluble Fe in Aerosols Sustained by Gaseous HO_2 Uptake. *Environmental Science & Technology Letters* **2017,** *4* (3), 98-104.

45. Bates, K. H.; Jacob, D. J.; Li, K.; Ivatt, P. D.; Evans, M. J.; Yan, Y.; Lin, J. Development and Evaluation of a New Compact Mechanism for Aromatic Oxidation in Atmospheric Models. *Atmospheric Chemistry and Physics* **2021,** *21* (24), 18351-18374.

46. Kwon, H. A.; Park, R. J.; Oak, Y. J.; Nowlan, C. R.; Janz, S. J.; Kowalewski, M. G.; Fried, A.; Walega, J.; Bates, K. H.; Choi, J.; Blake, D. R.; Wisthaler, A.; Woo, J. H. Top-down Estimates of Anthropogenic VOC Emissions in South Korea Using Formaldehyde Vertical Column Densities from Aircraft during the KORUS-AQ Campaign. *Elementa-Science of the Anthropocene* **2021,** *9* (1), 00109.

47. Kim, P. S.; Jacob, D. J.; Fisher, J. A.; Travis, K.; Yu, K.; Zhu, L.; Yantosca, R. M.; Sulprizio, M. P.; Jimenez, J. L.; Campuzano-Jost, P.; Froyd, K. D.; Liao, J.; Hair, J. W.; Fenn, M. A.; Butler, C. F.; Wagner, N. L.; Gordon, T. D.; Welti, A.; Wennberg, P. O.; Crounse, J. D.; St Clair, J. M.; Teng, A. P.; Millet, D. B.; Schwarz, J. P.; Markovic, M. Z.; Perring, A. E. Sources, Seasonality, and Trends of Southeast US Aerosol: An Integrated Analysis of Surface, Aircraft, and Aatellite Observations with the GEOS-Chem Chemical Transport Model. *Atmospheric Chemistry and Physics* **2015,** *15* (18), 10411-10433.

48. Pai, S. J.; Heald, C. L.; Pierce, J. R.; Farina, S. C.; Marais, E. A.; Jimenez, J. L.; Campuzano-Jost, P.; Nault, B. A.; Middlebrook, A. M.; Coe, H.; Shilling, J. E.; Bahreini, R.; Dingle, J.

H.; Vu, K. An Evaluation of Global Organic Aerosol Schemes Using Airborne Observations. *Atmospheric Chemistry and Physics* **2020,** *20* (5), 2637-2665.

49. Miao, R.; Chen, Q.; Zheng, Y.; Cheng, X.; Sun, Y.; Palmer, P. I.; Shrivastava, M.; Guo, J.; Zhang, Q.; Liu, Y.; Tan, Z.; Ma, X.; Chen, S.; Zeng, L.; Lu, K.; Zhang, Y. Model Bias in Simulating Major Chemical Components of $PM_{2.5}$ in China. *Atmospheric Chemistry and Physics* **2020,** *20* (20), 12265-12284.

50. Shah, V.; Jacob, D. J.; Li, K.; Silvern, R. F.; Zhai, S.; Liu, M.; Lin, J.; Zhang, Q. Effect of Changing NOx Lifetime on the Seasonality and Long-term Trends of Satellite-observed Tropospheric NO_2 Columns over China. *Atmospheric Chemistry and Physics* **2020,** *20* (3), 1483-1495.

51. Jaeglé, L.; Shah, V.; Thornton, J. A.; Lopez-Hilfiker, F. D.; Lee, B. H.; McDuffie, E. E.; Fibiger, D.; Brown, S. S.; Veres, P.; Sparks, T. L.; Ebben, C. J.; Wooldridge, P. J.; Kenagy, H. S.; Cohen, R. C.; Weinheimer, A. J.; Campos, T. L.; Montzka, D. D.; Digangi, J. P.; Wolfe, G. M.; Hanisco, T.; Schroder, J. C.; Campuzano-Jost, P.; Day, D. A.; Jimenez, J. L.; Sullivan, A. P.; Guo, H.; Weber, R. J. Nitrogen Oxides Emissions, Chemistry, Deposition, and Export Over the Northeast United States During the WINTER Aircraft Campaign. *Journal of Geophysical Research-Atmospheres* **2018,** *123* (21), 12368-12393.

52. Spataro, F.; Ianniello, A.; Esposito, G.; Allegrini, I.; Zhu, T.; Hu, M. Occurrence of Atmospheric Nitrous Acid in the Urban Area of Beijing (China). *Science of the Total Environment* **2013,** *447*, 210-224.

53. Finlayson-Pitts, B. J.; Wingen, L. M.; Sumner, A. L.; Syomin, D.; Ramazan, K. A. The Heterogeneous Hydrolysis of NO_2 in Laboratory Systems and in Outdoor and Indoor Atmospheres: An Integrated Mechanism. *Physical Chemistry Chemical Physics* **2003,** *5* (2), 223-242.

54. Gustafsson, R. J.; Kyriakou, G.; Lambert, R. M. The Molecular Mechanism of Tropospheric Nitrous Acid Production on Mineral Dust Surfaces. *Chemphyschem* **2008,** *9* (10), 1390-1393.

55. Fu, X.; Wang, T.; Gao, J.; Wang, P.; Liu, Y.; Wang, S.; Zhao, B.; Xue, L. Persistent Heavy Winter Nitrate Pollution Driven by Increased Photochemical Oxidants in Northern China. *Environmental Science & Technology* **2020,** *54* (7), 3881-3889.

56. Tian, R.; Ma, X.; Zhao, J. A Revised Mineral Dust Emission Scheme in GEOS-Chem: Improvements in Dust Simulations over China. *Atmospheric Chemistry and Physics* **2021,** *21* (6), 4319-4337.

57. Chuang, P. Y.; Duvall, R. M.; Shafer, M. M.; Schauer, J. J. The Origin of Water Soluble Particulate Iron in the Asian Atmospheric Outflow. *Geophysical Research Letters* **2005,** *32*, L07813.

58. Luo, C.; Mahowald, N.; Bond, T.; Chuang, P. Y.; Artaxo, P.; Siefert, R.; Chen, Y.; Schauer, J. Combustion Iron Distribution and Deposition. *Global Biogeochemical Cycles* **2008,** *22*, GB1012.

59. Sarwar, G.; Simon, H.; Xing, J.; Mathur, R. Importance of Tropospheric $ClNO_2$ Chemistry across the Northern Hemisphere. *Geophysical Research Letters* **2014,** *41* (11), 4050-4058.

60. Machulek, A.; Moraes, J. E. F.; Okano, L. T.; Silvério, C. A.; Quina, F. H. Photolysis of Ferric Ions in the Presence of Sulfate or Chloride Ions: Implications for the Photo-Fenton Process. *Photochemical & Photobiological Sciences* **2009,** *8* (7), 985-991.

61. Millero, F. J. Solubility of Fe(III) in Seawater. *Earth and Planetary Science Letters* **1998,** *154* (1-4), 323-329.

62. Craig, R. L.; Peterson, P. K.; Nandy, L.; Lei, Z.; Hossain, M. A.; Camarena, S.; Dodson, R. A.; Cook, R. D.; Dutcher, C. S.; Ault, A. P. Direct Determination of Aerosol pH: Size-Resolved Measurements of Submicrometer and Supermicrometer Aqueous Particles. *Analytical Chemistry* **2018,** *90* (19), 11232-11239.

63. Fang, T.; Guo, H.; Zeng, L.; Verma, V.; Nenes, A.; Weber, R. J. Highly Acidic Ambient Particles, Soluble Metals, and Oxidative Potential: A Link between Sulfate and Aerosol Toxicity. *Environmental Science & Technology* **2017,** *51* (5), 2611-2620.

64. Tao, W.; Su, H.; Zheng, G.; Wang, J.; Wei, C.; Liu, L.; Ma, N.; Li, M.; Zhang, Q.; Pöschl, U.; Cheng, Y. Aerosol pH and Chemical Regimes of Sulfate Formation in Aerosol Water during Winter Haze in the North China Plain. *Atmospheric Chemistry and Physics* **2020,** *20* (20), 11729-11746.

65. Zhang, L.; Chen, Y.; Zhao, Y.; Henze, D. K.; Zhu, L.; Song, Y.; Paulot, F.; Liu, X.; Pan, Y.; Lin, Y.; Huang, B. Agricultural Ammonia Emissions in China: Reconciling Bottom-up and Top-down Estimates. *Atmospheric Chemistry and Physics* **2018,** *18* (1), 339-355.

66. Abbatt, J. P. D.; Waschewsky, G. C. G. Heterogeneous Interactions of HOBr, HNO_3, O_3, and NO_2 with Deliquescent NaCl Aerosols at Room Temperature. *Journal of Physical Chemistry A* **1998,** *102* (21), 3719-3725.

67. Sadanaga, Y.; Hirokawa, J.; Akimoto, H. Formation of Molecular Chlorine in Dark Condition: Heterogeneous Reaction of Ozone with Sea Salt in the Presence of Ferric Ion. *Geophysical Research Letters* **2001,** *28* (23), 4433-4436.

68. Faxon, C. B.; Dhulipala, S. V.; Allen, D. T.; Hildebrandt Ruiz, L. Heterogeneous Production of Cl_2 from Particulate Chloride: Effects of Composition and Relative Humidity. *AIChE Journal* **2018,** *64* (8), 3151-3158.

69. Liu, H. J.; Zhao, C. S.; Nekat, B.; Ma, N.; Wiedensohler, A.; Van Pinxteren, D.; Spindler, G.; Müller, K.; Herrmann, H. Aerosol Hygroscopicity Derived from Size-segregated Chemical Composition and Its Parameterization in the North China Plain. *Atmospheric Chemistry and Physics* **2014,** *14*(5), 2525-2539.

70. Petters, M. D.; Kreidenweis, S. M. A Single Parameter Representation of Hygroscopic Growth and Cloud Condensation Nucleus Activity. *Atmospheric Chemistry and Physics* **2007,** *7*, 1961–1971.

71. Choi, M.S.; Qiu, X.; Zhang, J.; Wang, S.; Li, X.; Sun, Y.; Chen, J.; Ying, Q. Study of Secondary Organic Aerosol Formation from Chlorine Radical-initiated Oxidation of Volatile

Organic Compounds in a Polluted Atmosphere using a 3D Chemical Transport Model. *Environmental Science & Technology* **2020,** *54*(21), 13409-13418.

72. Li, Q.; Fernandez, R. P.; Hossaini, R.; Iglesias-Suarez, F.; Cuevas, C. A.; Apel, E. C.; Kinnison D. E.; Lamarque, J. F.; Saiz-Lopez, A. Reactive Halogens Increase the Global Methane Lifetime and Radiative Forcing in the 21st Century. *Nature Communications* **2022,** *13*, 2768.

73. Li, Q.; Meidan, D.; Hess, P.; Añel, J. A.; Cuevas, C. A.; Doney, S.; Fernandez, R. P.; van Herpen, M.; Höglund-Isaksson, L.; Johnson, M. S.; Kinnison, D. E.; Lamarque, J.-F.; Röckmann, T.; Mahowald, N. M.; Saiz-Lopez, A. Global Environmental Implications of Atmospheric Methane Removal through Chlorine-mediated Chemistry-climate Interactions. *Nature Communications* **2023,** *14*, 4045.

74. Mikkelsen, M. K.; Liisberg, J. B.; van Herpen, M. M. J. W.; Mikkelsen, K. V.; Johnson, M. S. Photocatalytic Chloride-to-chlorine Conversion by Ionic Iron in Aqueous Aerosols: a Combined Experimental, Quantum Chemical, and Chemical Equilibrium Model Study. *Aerosol Research* **2024,** *2*, 31-47.

75. De Laat, J.; Le, T.G. Kinetics and Modeling of the Fe(III)/H_2O_2 System in the Presence of Sulfate in Acidic Aqueous Solutions. *Environmental Science & Technology* **2005,** *39*(6), 1811-1818.

76. Gen, M.; Liang, Z.; Zhang, R.; Mabato, B. R. G.; Chan, C. K. Particulate Nitrate Photolysis in the Atmosphere. *Environmental Science: Atmospheres* **2022,** *2*(2), 111-127.

77. Zhao, S.; Hu, B.; Liu, H.; Du, C.; Xia, X.; Wang, Y. The Influence of Aerosols on the NO_2 Photolysis Rate in a Suburban Site in North China. *Science of the Total Environment* **2021,** *767*, 144788.

78. Moorhead, E. G.; Sutin, N. Rate and Equilibrium Constants for the Formation of the Monooxalate Complex of Iron(III). *Inorganic Chemistry* **1966,** *5*, 1866−1871.

79. Mentasti, E.; Pelizzetti, E. Reactions Between Iron(III) and Catechol (o-Dihydroxybenzene). Part I. Equilibria and Kinetics of Complex Formation in Aqueous Acid Solution. Journal of the Chemical Society, Dalton Transactions **1973,** *23*, 2605−2608.

80. Herrmann, H.; Schaefer, T.; Tilgner, A.; Styler, S. A.; Weller, C.; Teich, M.; Otto, T. Tropospheric Aqueous-phase Chemistry: Kinetics, Mechanisms, and its Coupling to a Changing Gas Phase. *Chemical Reviews* **2015,** *115*(10), 4259-4334.

81. Lei, Y.; Lei, X.; Westerhoff, P.; Zhang, X.; Yang, X. Reactivity of Chlorine Radicals (Cl• and Cl_2•–) with Dissolved Organic Matter and the Formation of Chlorinated Byproducts. *Environmental Science & Technology* **2020,** *55*(1), 689-699.

847 For Table of Contents Only

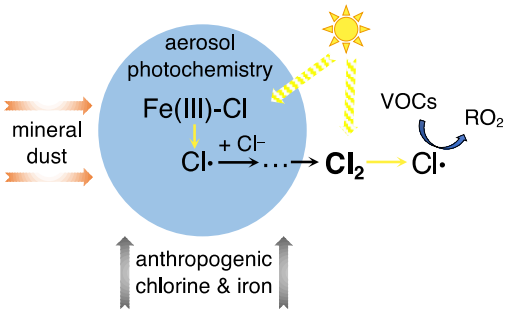

848

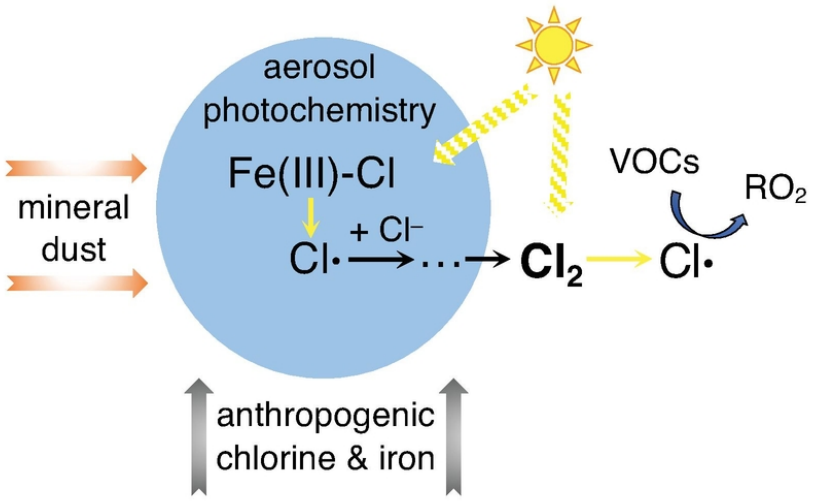

For Table of Contents Only

82x44mm (300 x 300 DPI)